CHEMISTRY
A European Journal

A Journal of
ChemPubSoc Europe

Accepted Article

Title: The effect of guest metal ions on the reduction potentials of uranium(VI) complexes: Experimental and theoretical investigations

Authors: Tanmoy Kumar Ghosh, Prithwish Mahapatra, Michael G. B. Drew, Antonio Franconetti, Antonio Frontera, and Ashutosh Ghosh

To be cited as: *Chem. Eur. J.* 10.1002/chem.201904253

Link to VoR: http://dx.doi.org/10.1002/chem.201904253

Supported by
ACES

WILEY-VCH

10.1002/chem.201904253

The effect of guest metal ions on the reduction potentials of uranium(VI) complexes: Experimental and theoretical investigations

Tanmoy Kumar Ghosh,[a] Prithwish Mahapatra,[a] Michael G. B. Drew,[b] Antonio Franconetti,[c] Antonio Frontera,[c]* Ashutosh Ghosh[a]*

[a]*Department of Chemistry, University College of Science, University of Calcutta, 92, A.P.C. Road, Kolkata 700 009, India, E-mail address: ghosh_59@yahoo.com*

[b]*School of Chemistry, The University of Reading, P.O. Box 224, Whiteknights, Reading RG6 6AD, United Kingdom*

[c]*Departament de Química, Universitat de les Illes Balears, Crta de Valldemossa km 7.5, 07122 Palma de Mallorca (Baleares), SPAIN, E-mail: toni.frontera@uib.es*

Abstract

Two mononuclear uranyl complexes, $[UO_2L^1]$ (**1**) and $[UO_2L^2]\cdot CH_3CN\cdot CH_3OH$ (**2**) have been synthesized from two multidentate N_3O_4 donor ligands, *N*,*N*′-bis(5-methoxysalicylidene)diethylenetriamine (H_2L^1) and *N*,*N*′-bis(3-methoxysalicylidene)diethylenetriamine (H_2L^2) and structurally characterized. Both complexes showed a reversible U(VI)/U(V) couple at −1.571 and −1.519 V respectively, in cyclic voltammetry. The reduction potential of the U(VI)/U(V) couple shifted towards more positive potential on addition of Li^+, Na^+, K^+ and Ag^+ metal ions to the acetonitrile solution of complex **2** and the resulting potential was correlated with the Lewis acidity of the metal ions and was also justified by theoretical DFT calculations. No such shift in reduction potential was observed for complex **1**. All four bimetallic products, $[UO_2L^2Li_{0.5}](ClO_4)_{0.5}$ (**3**), $[UO_2L^2Na(ClO_4)]_2$ (**4**), $[UO_2L^2Ag(NO_3)(H_2O)]$ (**5**) and $[(UO_2L^2)_2K(H_2O)_2]PF_6$ (**6**), formed on addition of the Li^+, Na^+, Ag^+ and K^+ metal ions, respectively, to acetonitrile solution of complex **2**, were isolated in solid state and structurally characterized by single crystal X-ray diffraction. In all the species, the inner N_3O_2 donor set of the ligand encompasses the equatorial plane of uranyl ion and the outer open compartment with $O_2O'_2$ donor sites hosts the second metal ion.

Introduction

The redox behavior of transition metal complexes is extremely important for their reactivity and efficiency towards various catalytic oxidation/reduction, polymerization and coupling reactions.[1-4] It has been found that in many cases, the presence of a specific redox-inactive metal ion is crucial for the functioning of various naturally occurring enzymes.[5-7] For example, the Ca^{2+} ion is vital for oxo-bridged tetra-manganese based enzyme in Photosystem II (PS II) which oxidizes water to generate molecular oxygen.[8-11] The Sr^{2+} substituted PS II can also provide oxygen evolution, but on substitution by several other cations, like Cd^{2+}, its oxygen evolving activity is lost, indicating that not only the charge but also Lewis acidity of metal ions may be a key factor for its reactivity.[12-16] Inspired by the observation in natural enzymes and the utility of redox-inactive metal ions, several groups have synthesized bimetallic Ni(II), Co(II), Fe(II/III), Mn(II/III) complexes with various Lewis acidic metal ions, like Li^{+}, Na^{+}, K^{+}, Ca^{2+}, Sr^{2+} etc.[12][17-20] The electrochemical properties of these complexes are widely studied and a relationship between the Lewis acidity of redox-inactive metal ions and the reduction potential of corresponding hetro-bimetallic complex is established.[17-20] The difference in electron withdrawing ability of these redox-inactive metal ions leads to the modification in ligand field around the redox-active metal ions which would result in the considerable amendment in electronic structure as well as shifting of redox potential. Till date, these studies are performed by using bimetallic transition metal complexes, but our objective is to extend these studies to actinide metals such as uranium.

The interest of coordination complexes of uranium in current research is growing due to their significant photoluminescent, photocatalytic, electrochemical, optical and molecular magnetic properties.[21-27] The studies of these properties of uranium are helpful for waste management in nuclear reactors to prevent water and soil pollution. Uranium forms stable complex with multidentate organic ligands, a fact which is exploited in the detection and separation of uranium from nuclear slag, ground and seawater.[28-31] It shows multiple oxidation states, varying from +III to +VI but in aerobic condition, the common oxidation state is +VI which is stabilized as the uranyl dication (UO_2^{2+}).[32-39] A convenient method for synthesis of U(V) compound is to reduce the corresponding U(VI) species electrochemically.[40-43] Several complexes of U(V) with N_2O_2 donor salen type Schiff bases have been prepared by this method. In these complexes, the N_2O_2 donor set along with a solvent molecule form the pentagonal basal plane around U with two axial oxygen

atoms.[42,43] Such U(VI) compounds usually show a reversible redox cycle at a potential around –1.6 V (*vs.* Fc^+/Fc) which is susceptible to the donor atoms of coordinated ligands and the solvent environment.[43]

Diamines such as 1,2-ethanediamine or 1,3-propanediamine readily undergo 1:2 condensation with *o*-vaniline to produce a group of bi-compartmental ligands which have been used extensively for the synthesis of phenoxido bridged heterometallic complexes.[44-45] The inner compartment of such a ligand hosts a 3d metal ion through the coordination of N_2O_2 donor set of atoms whereas the open $O_2O'_2$ compartment accommodates various oxophilic cations including lanthanides.[44-47] Such ligands are known to coordinate to uranyl ion through the N_2O_2 donor set but do not behave as a compartmental ligand presumably due to the bigger size and preference for penta coordination around the basal plane of uranium. On the other hand, the Schiff base formed by the 1:2 condensation of diethylenetriamine and *o*-vaniline is expected to be well-suited to host a uranyl ion in its inner N_3O_2 donor compartment[41] while the outer $O_2O'_2$ donor set remains suitably positioned to coordinate to a second metal ion.

In the present work, we have synthesized two ligands, *N*,*N*′-bis(5-methoxysalicylidene)diethylenetriamine (H_2L^1) and *N*,*N*′-bis(3-methoxysalicylidene)diethylenetriamine (H_2L^2) and their mononuclear U(VI) complexes $[UO_2L^1]$ (**1**) and $[UO_2L^2]\cdot CH_3CN\cdot CH_3OH$ (**2**). The electrochemical properties of these complexes are studied by cyclic voltammetric measurements. A substantial shift of the reduction potential of U(VI)/U(V) couple is observed upon addition of Li^+, Na^+, K^+ and Ag^+ metal ions to the acetonotrile solution of complex **2** and these shifts have been rationalized considering the Lewis acidity of the respective metal ions and also by theoretical DFT calculations. The bimetallic complexes, $[UO_2L^2Li_{0.5}](ClO_4)_{0.5}$ (**3**), $[UO_2L^2Na(ClO_4)]_2$ (**4**), $[(UO_2L^2)_2K(H_2O)_2]PF_6$ (**6**), and $[UO_2L^2Ag(NO_3)(H_2O)]$ (**5**) have also been synthesized by reacting complex **2** with Li^+, Na^+, K^+ and Ag^+ metal ions, respectively and characterized by single crystal X-ray diffraction. The existence of these species in solution phase is confirmed by ESI-mass spectral analyses. It is to be mentioned here that this is the first study where the shift of the reduction potential of U(VI)/U(V) couple by the influence of a second metal ion is investigated.

10.1002/chem.201904253

Results and discussion

Syntheses of the complexes

The polydentate Schiff base ligands, H_2L^1 and H_2L^2 were prepared by 1:2 condensations of diethylenetriamine and 5-methoxysalicylaldehyde and *o*-vanillin, respectively in methanol. These ligands (H_2L^1 and H_2L^2) were reacted with the $UO_2(NO_3)_2{\cdot}6H_2O$ in 1:1 molar ratio at room temperature to form new mononuclear complexes $[UO_2L^1]$ (**1**) and $[UO_2L^2]{\cdot}CH_3CN{\cdot}CH_3OH$ (**2**), respectively. When complex **2** was reacted with $Li(ClO_4){\cdot}6H_2O$, $Na(ClO_4)_2$, $AgNO_3$ and KPF_6 in 1:1 molar ratio at room temperature in acetonitrile solution, hetero-bimetallic complexes, $[UO_2L^2Li_{0.5}](ClO_4)_{0.5}$ (**3**), $[UO_2L^2Na(ClO_4)]_2$ (**4**), $[UO_2L^2Ag(NO_3)(H_2O)]$ (**5**) and $[(UO_2L^2)_2K(H_2O)_2]PF_6$ (**6**), respectively were separated out as crystalline products. On the other hand, the same reaction with complex **1** did not yield any such bimetallic complex; instead complex **1** itself separated out on slow evaporation of the solvent. The syntheses of complexes **1**–**6** are depicted in Scheme 1.

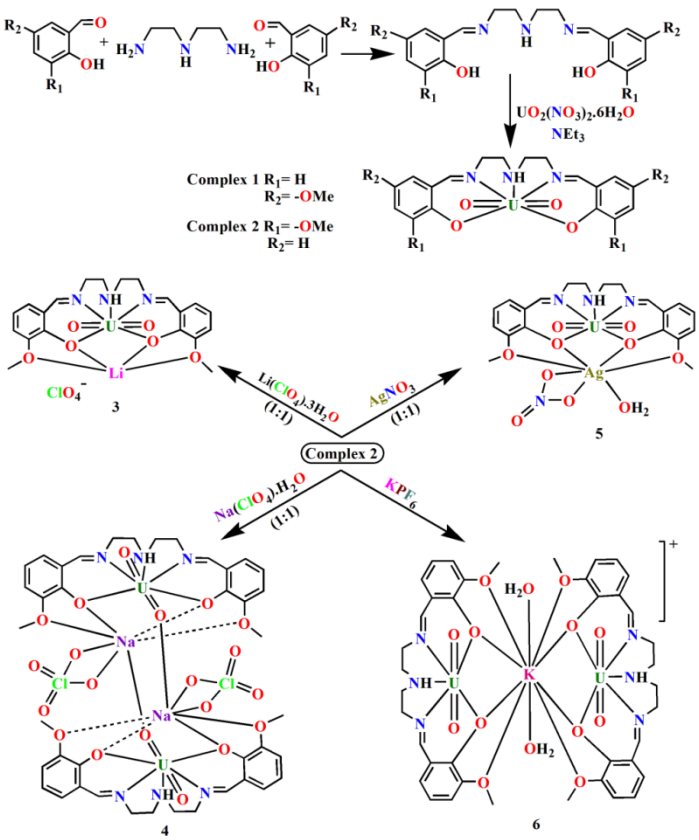

Scheme 1: Syntheses of complexes **1**–**6**.

IR spectra of complexes

In the IR spectra of all complexes **1**−**6**, there is a strong and sharp band at around 1630 cm^{-1} due to the stretching of azomethine ν(C=N) group of the Schiff base ligand (Figures S1−S6, Supporting Information) and at around 890 cm^{-1} for asymmetric stretching of uranyl (UO_2) group. Another strong and sharp band is observed in the IR spectra of all these complexes in the range of 3186−3248 cm^{-1} for the stretching of N−H group in the Schiff base ligand. Here, the N−H stretching in all the complexes is in lower frequency than that in free ligand (3343 cm^{-1}) which indicate the possibility of H-bonding. A strong band at around 1080 cm^{-1} for complexes **3** and **4** indicates the presence of the perchlorate anion. In the IR spectra of complex **5**, the presence of the nitrate anion is evident from a strong sharp band at 1384 cm^{-1}. The characteristic IR band for hexafluorophosphate anion in complex **6** is observed at around 845 cm^{-1}.

Electronic spectroscopy

Electronic spectra of all complexes **1**−**6**, were recorded in acetonitrile solvent (Figures S7, Supporting Information). The spectrum of $[UO_2L^1]$ exhibits one band at 368 nm in acetonitrile whereas that of $[UO_2L^2]$ shows two bands at 410 and 264 nm. These bands are due to ligand to metal charge transfer transitions. On the other hand, complexes **3**−**6** show two absorption bands at 395, 267 nm for complex **3**; 400, 266 nm for complex **4**; 400, 267 nm for complex **5** and 397, 268 nm for complex **6** for ligand to metal charge transfer.

ESI-Mass Spectrometric Study

ESI-mass spectra of all complexes **1**−**6** were recorded in acetonitrile solution, which are shown in Figures S8−S13, Supporting Information. In these spectra, the base peaks are observed at *m/z* = 640.45 (calcd 640.22) for $[UO_2L^1 + H]^+$, 662.21 (calcd 662.20) for $[UO_2L^2 + Na]^+$, 646.23 (calcd 646.23) for $[UO_2L^2 + Li]^+$, 662.20 (calcd 662.20) for $[UO_2L^2 + Na]^+$, 746.12 (calcd 746.11) for $[UO_2L^2 + Ag]^+$ and 678.58 (calcd 678.17) for $[UO_2L^2 + K]^+$ for complexes **1**−**6**, respectively. In case of complexes **1** and **2**, the base peak appeared due to H^+ and Na^+ adducts of these complexes, respectively. Whereas, in complexes **3**−**6** the base peaks correspond only to the respective bimetallic species.

^{1}H NMR Study

^{1}H NMR spectra of all complexes **1**−**6** and complex **2** + Li^+ were recorded in CD_3CN solution (Figures S14−S20, Supporting Information). In these spectra, slight downfield shift for the signals correspond to the aromatic protons of the ligand was observed for all the bimetallic complexes **3**−**6** compared to that of complex **2**. These results are expected as the incorporation of Lewis acidic metal ions leads to the withdrawal of the electron density from the [UO_2L^2] and thus enhances the deshielding of aromatic protons resulting in a downfield shift. The ^{1}H NMR spectra of complex **3** show doublet of doublets for two aromatic protons, similar to that in complex **2**, except that these peaks are shifted to the downfield region. However, on the addition of eqiumolar amount of Li^+ ion to complex **2**, these doublets shift even more downfield with less pronounced splitting (Figure S21 in Supporting Information) like those of complexes **4** and **6**.

Description of structures

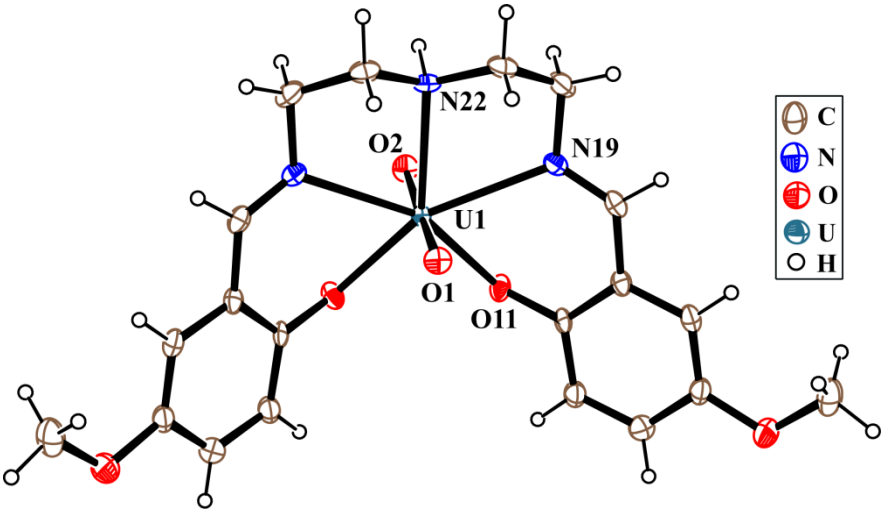

Figure 1.The structure of **1** which has crystallographic mirror symmetry with ellipsoids shown at 30% probability.

The structure of **1**, UO_2L^1 which has crystallographic mirror symmetry is shown in Figure 1 together with the atomic numbering scheme in the coordination sphere.

In **1**, the metal atom is seven-coordinate with a pentagonal bipyramidal environment being bonded to two terminal oxygen atoms in axial positions and the five donor atoms of the ligand in the equatorial plane. The two terminal oxygen atoms are 1.748(6), 1.768(6) Å from the metal with a O-U-O angle of 177.2(3)^o while in the equatorial plane, unique distances are

10.1002/chem.201904253

U-N 2.561(5), 2.579(7) Å and U-O 2.210(4) Å. These five atoms show a r.m.s. deviation of 0.133 Å with the metal atom 0.035(3) Å from the plane. However the ligand is severely bent and the two aromatic rings intersect at an angle of 63.1(1)°. Selected bond lengths and bond angles of complex **1** are given in Table S1 (Supporting Information). The unique nitrogen atom N22 forms a weak intermolecular hydrogen bond to a terminal oxygen O2$1 ($1 = x+½, y, ½-z) with dimensions shown in Table S4 (Supporting Information).

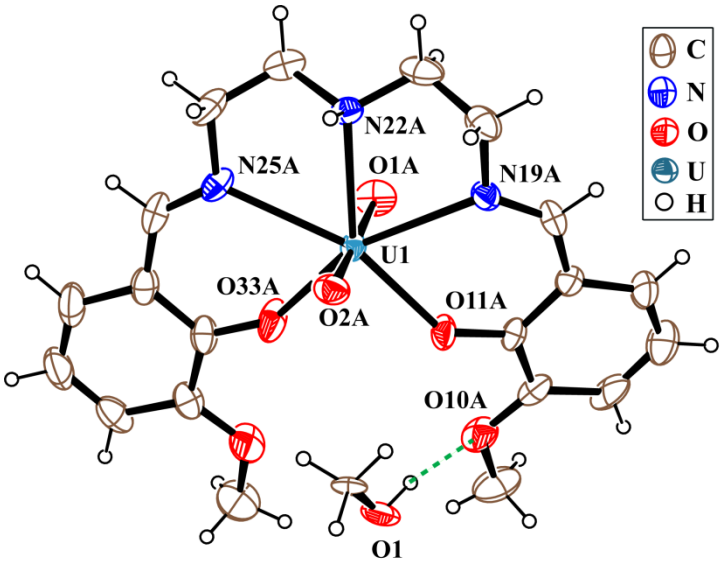

Figure 2. The structure of **2A** with ellipsoids at 30% probability. The structure of **2B** is similar though there is no solvent molecule in the cavity. The methanol solvent molecule is refined with 50% occupancy. Dotted line shows the hydrogen bonding.

In complex **2** there are two molecules of UO_2L^2 in the asymmetric unit together with solvent molecules of MeCN and MeOH, the latter being refined with 50% occupancy. The two molecules show approximate mirror symmetry though not crystallographically imposed. The two UO_2L^2 molecules, named A, shown in Figure 2, and B have equivalent structures. The difference between L^2 with the -OMe in an ortho position in **2** compared to L^1 with the -OMe in a para position in **1** facilitates the formation of a cavity adjacent to the uranyl atom though there is no significant interaction between the -OMe groups and the uranium. However unlike structures, **3**, **4** and **5** the cavity is not filled with an additional metal. In molecule A there is a solvent methanol molecule refined with 50% occupancy which forms a hydrogen bond O1-H…O10 (dimensions in Table S4 (Supporting Information) but this solvent molecule remains well above the plane of the cavity. There is no such solvent interaction with molecule B. The geometry around the uranium atoms in molecules A and B is very similar to that found in **1**.

10.1002/chem.201904253

The r.m.s. deviations of the five donor atoms in the equatorial planes are 0.031, 0.103 Å with the metal 0.037(5), 0.010(4) Å respectively from the plane. However, there are significant differences in the conformation of the ligand in A and B. For example, the two aromatic rings intersect at 19.2(7)^{o} in A and 50.5(4)^{o} in B and in A, O10 and O34 are 0.72(2), 0.02(2) Å and in B 0.24(2), 0.40(2) Å from the equatorial plane. Selected bond lengths and bond angles of complex **2** are given in Table S2 (Supporting Information). In both A and B, N22 forms an intermolecular donor hydrogen bond to a terminal oxygen atom, details in Table S4 (Supporting Information).

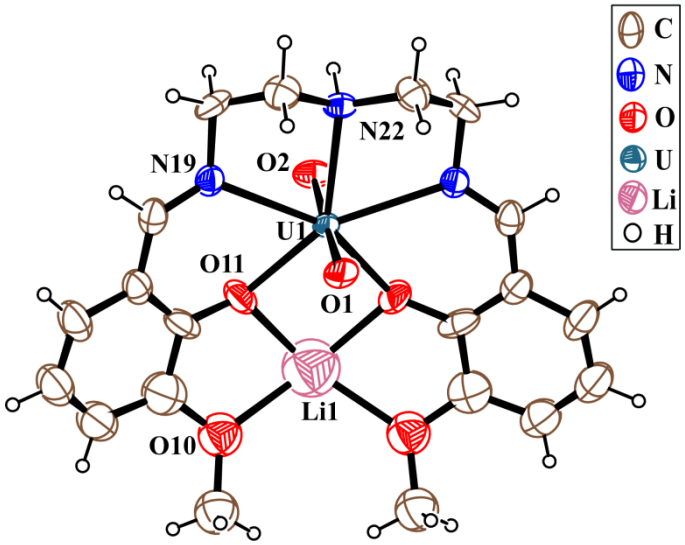

Figure 3.The structure of **3** which contains crystallographic mirror symmetry with ellipsoids at 30% probability.

The structure of **3** which has crystallographic mirror symmetry is shown in Figure 3. The complex contains UO_2L^2 with the same basic structure as in **2**, but in this structure the cavity is occupied by a lithium ion. The charge is balanced by a disordered perchlorate anion. As the chlorine was in a special position, the maximum possible amount of $Li(ClO_4)$ per uranium complex was 0.5 and it was decided to refine with this value although reduced occupancy is feasible. In addition the perchlorate oxygen atoms were disordered over several positions. The geometry of the uranium coordination sphere was similar to that found in **1** and **2**. In the pentagonal bipyramid the five donor atoms in the equatorial plane show a r.m.s. deviation of 0.071 Å with the uranium atom 0.052(8) Å from the plane. The two aromatic rings intersect at an angle of 47.1(7)^{o}. The Li ion forms bonds to O10 and O11 and the symmetry equivalents but O10 is disordered over two positions so it is difficult to assess the exact

10.1002/chem.201904253

coordination geometry around the Li ion. Selected bond lengths and bond angles of complex **3** are given in Table S1 (Supporting Information). As in other structures, N22 forms a intermolecular donor hydrogen bond to a terminal oxygen atom, O1 (3/2-x, ½-y, z+1/2) details in Table S4 (Supporting Information).

.

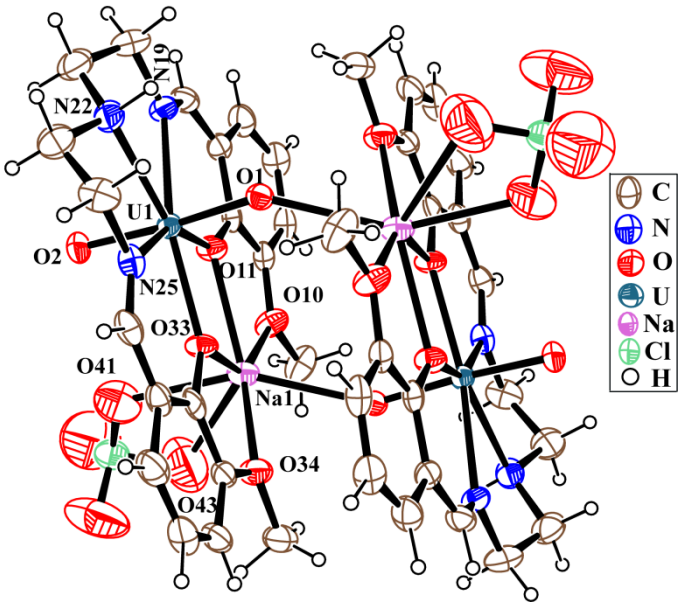

Figure 4. The dimeric structure $(UO_2L^2NaClO_4)_2$ of complex **4** with ellipsoids at 30% probability.

The structure of **4** which contains no crystallographic symmetry is shown in Figure 4. Here the basic structure is the same as that of **3** but with a sodium ion in the cavity. The geometry of the UO_2L^2 moiety is similar to that found in the other structures. The atoms in the equatorial plane show a r.m.s. of 0.045 Å with the metal 0.006(4) Å from the plane. However in this structure the two aromatic planes are closely planar with an intersecting angle of 3.4(9)^o. This is clearly a consequence of the strong binding to the sodium ion in the cavity and the formation of a dimer. The four oxygen atoms of the ligand O10, O11, O33, O34 are bonded to the sodium at distances of 2.299(10), 2.449(9), 2.431(9), 2.303(10) Å with a r.m.s. deviation of 0.062 Å from a plane from which the sodium deviates by 0.115(6) Å. In addition to these bonds the sodium is bonded to two oxygen atoms of the perchlorate O41 and O43 at 2.50(2), 2.70(2) Å and to a terminal oxygen atom O1 (1-x, 2-y, 2-z) at 2.568(10) Å. This latter bond creates a dimeric structure as shown in Figure 4. Selected bond lengths and bond angles of complex **4** are given in Table S3 (Supporting Information). As in the other

10.1002/chem.201904253

structures N22 forms an intermolecular donor hydrogen bond, but in this case to a perchlorate oxygen atom, details in Table S4 (Supporting Information).

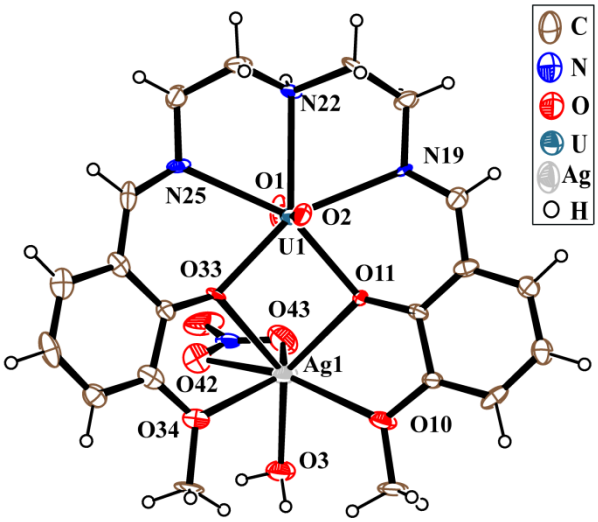

Figure 5. The structure of **5** with ellipsoids at 30% probability.

In the structure of **5**, which has no imposed symmetry, the metal in the cavity is silver but it is too large to fit readily into the cavity (shown in Figure 5). As a result the ligand deviates far more from planarity than in complex **4**. The r.m.s. deviation of the five donor atoms in the equatorial plane is 0.120 Å and the uranium atom is 0.034(7) Å from the plane. The two aromatic planes intersect at 52.9(7)^{o}. For the silver coordination sphere, the r.m.s. deviation of the four oxygen atoms in the ligand is 0.034 Å with the metal is 1.417(8) Å from the plane. The silver atom is also bonded to a water molecule O3 at 2.352(15) Å and two oxygen atoms of a nitrate ligand O(42) at 2.60(2) Å and O43 at 2.65(2) Å. If the nitrate is considered as one bonding site, then the geometry around the silver atom is best described as a trigonal prism. Selected bond lengths and bond angles of complex **5** are given in Table S3 (Supporting Information). In this structure N22 forms an intermolecular hydrogen bond to a nitrate oxygen atom while the water molecule O3 forms hydrogen bonds to a terminal oxygen atom O1, details in Table S4 (Supporting Information).

We could not establish the structure of **6** in controvertibly from the X-ray data due to disorder but a likely structure containing a potassium ion on a center of symmetry sandwiched between two UO_2L^2 moieties was established and is shown as (Figure S22, Supporting Information).

10.1002/chem.201904253

Electrochemistry

Cyclic voltammograms (CVs) of complexes **1** and **2** were recorded in acetonitrile with respect to a ferrocene/ferrocenium ($Fc^{0/+}$) electrode at different scan rates. For complexes **1** and **2**, the peaks are observed at E_c= −1.604 and −1.560 V on forward cathodic scan for reduction process at electrode surface, whereas on reverse scan, anodic peaks are observed at E_a= −1.538 and −1.478 V, respectively at 100 mVs^{-1} scan rate. The peak separation values ($\Delta E_{pc} = E_{cathodic} - E_{anodic}$) are −0.066 and −0.082 V with the $E_{1/2}$ values of −1.571 and −1.519 V for complexes **1** and **2**, respectively (Figure 6). The reduction processes for both **1** and **2** are nearly reversible, and the appearance of peaks are due to the reduction of U(VI) to U(V) in the uranyl complexes. Another very small peak is observed for both complexes **1** and **2** at higher scan rates prior to the reduction potential of U(VI/V) couple. For complex **2** which is possibly due to the presence of little amount of impurity (Na^+ ion or other impurity) from the reference Ag/AgCl electrode. But for complex **1**, a small peak appear may be for other reasons as it does not form complex with Na^+. It is to be noted that this feature is less pronounced for **1** compared to **2**. Such small feature for the reduction of other U(VI) complexes has also been observed by other group and has been ascribed to the presence of small "unknown impuritiy".[26] After the addition of equimolecular redox inactive mono-positive metal ions in the solution of complex **2**, the cyclic voltammograms of mixtures are recorded. In these cyclic voltammograms the corresponding reduction potentials of U(VI) are observed at more positive potential than that of complex **2**. The peaks are observed at E_c = −1.328, −1.391 and −1.436 V on forward scan after the addition of Li^+, Na^+ and K^+, respectively. On reverse scan the corresponding anodic peaks are appeared at E_a = −1.242, −1.261 and −1.341 V. Peak separation values (ΔE_{pc}) are −0.086, −0.130 and −0.095 V with the $E_{1/2}$ values of −1.285, −1.326 and −1.388 V for the mixture of complex **2** with Li^+, Na^+ and K^+, respectively as shown in Figure 7 and Figures S23−S25 (Supporting Information). In these complexes a considerable shift in the reduction potential of U(VI/V) couple is observed. The shifts of $E_{1/2}$ values with respect to complex **2** are −0.234, −0.193 and −0.131 V for Li^+, Na^+ and K^+, respectively Table S5 (Supporting Information). On the contrary, the cyclic voltammograms of complex **2** show two peaks on forward scan at E_c= −1.361 and −1.541 V after the addition of redox active Ag^+ metal ion and on reverse scan the anodic peaks appear at E_a = −1.287 and −1.472 V. Here the peak separation values (ΔE_{pc}) are −0.074 and −0.069 V with the $E_{1/2}$ values of −1.324 and −1.507 V, respectively. Electrochemical data of all the

complexes are listed in Table S6 (Supporting Information). The peak at $E_{1/2}$ = −1.507 V is due to the U(VI/V) reduction couple, which is closer to the $E_{1/2}$value of complex **2** as shown in Figure 7 and S26 (Supporting Information). This peak indicates that some [UO_2L^2] species are free from silver in solution, whereas the other peak at $E_{1/2}$ = −1.324 V is due to the reduction of U(VI) to U(V) in the bimetallic Ag-U complex. The Ag^+ ion starts to reduce at a potential of −0.01 V and therefore some of Ag^+ ions get reduced during the potential scan producing the free [UO_2L^2] species as shown in S27 (Supporting Information). The higher cathodic current of the Ag-U complex compared to the others indicates that this reduction process is continuing during the scanning process. In the mixture of complex **2** and second metal ions (Li^+, Na^+, and K^+) the shift in reduction potential of U(VI/V) couple towards the lower potential range as shown in Figure 8, indicates the presence of cation coordinated [UO_2L^2] species in the solution, which is also confirmed from ESI-mass spectrometry. The differential pulse voltammograms of the complex **2** and a mixture of complex **2** with the guest metal ions Li^+, Na^+ or K^+ also show the similar change of potential as shown in Figure 8. In these hetero-bimetallic complexes the anodic shift in reduction potential of the U(VI) can be correlated with the Lewis acidity of the cations. The variation in reduction potential of U(VI/V) couple with the Lewis acidity of the cations is shown in Figure 9. The plot of $E_{1/2}$ values of U(VI/V) couple with the pK_a values of Li^+, Na^+ and K^+ metal ions shows a linear relationship, in which the reduction potential of uranium decreases with the decrease in pK_a values of the metal ions.[48,49] The electronic structure of the complexes as well as the redox potential of U(VI) is changed by the addition of guest metal ions to the neutral metalloligand (complex **2**). Therefore, all the complexes are energetically characterized for better understanding about the shift in reduction potential of the U(VI) in these complexes. The electrochemical measurements in the acetonitrile solution of complexes **4**−**6** show very similar results as described above by the addition of equimolecular mono-positive metal ions for Na^+, Ag^+ and K^+, respectively to the solution of complex **2**. However, complex **3** shows an additional peak at −1.528 V (Figure S28 in Supporting Information) which is not observed when equimolecular Li^+ ion is added to the solution of complex **2**. The position of this additional peak indicates the presence of free [UO_2L^2] species in the solution confirming that the occupancy of Li^+ ion is less than one as observed in the X-ray structure.

Although there are several reports of Schiff base complexes with an appended crown functionality and their wide utility towards electro-redox, we have shown here for the first

time that a common bi-compartmental Schiff base ligand can also be very useful to study the effect of a second metal ion on the reduction potential of the U(VI)/U(V) couple.

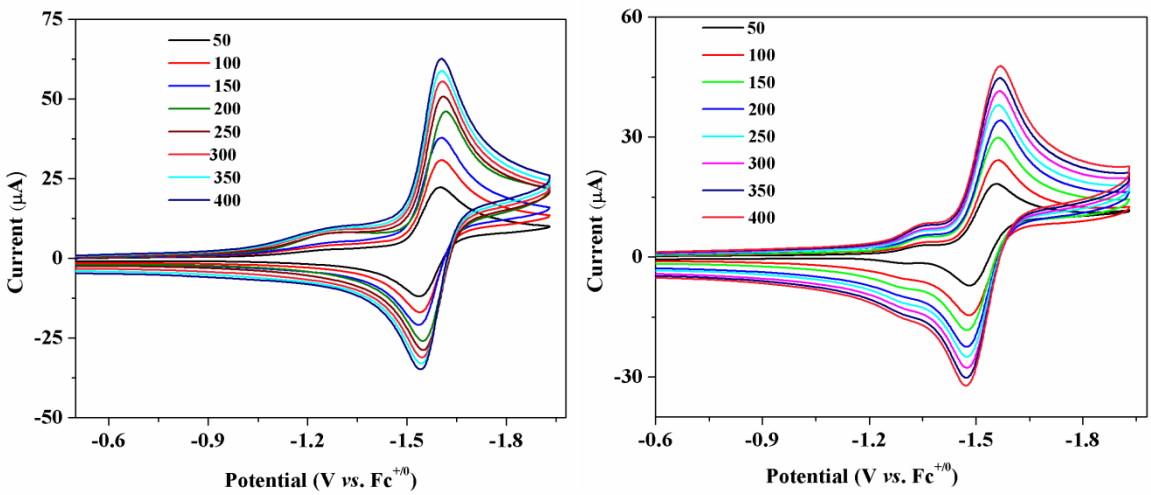

Figure 6. Cyclic voltammograms of complexes **1** (left) and **2** (right) which are recorded in acetronitrile (0.1 M TBAP) with a glassy carbon working electrode at different scan rate.

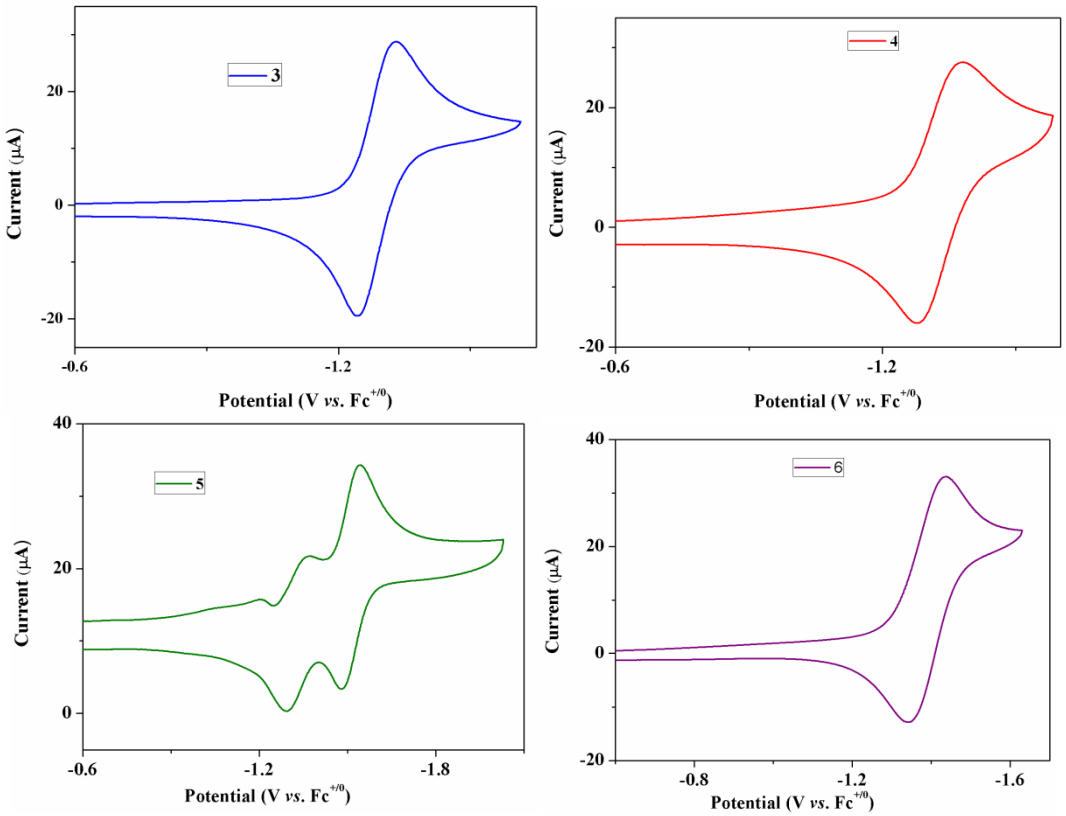

10.1002/chem.201904253

Figure 7. Cyclic voltammograms of $UO_2L^2 + M^+$ [M^+ = Li^+(**3**), Na^+(**4**), Ag^+(**5**), K^+(**6**)] which are recorded in acetonitrile (0.1 M TBAP) with a glassy carbon working electrode at 100 mVs^{-1} scan rate.

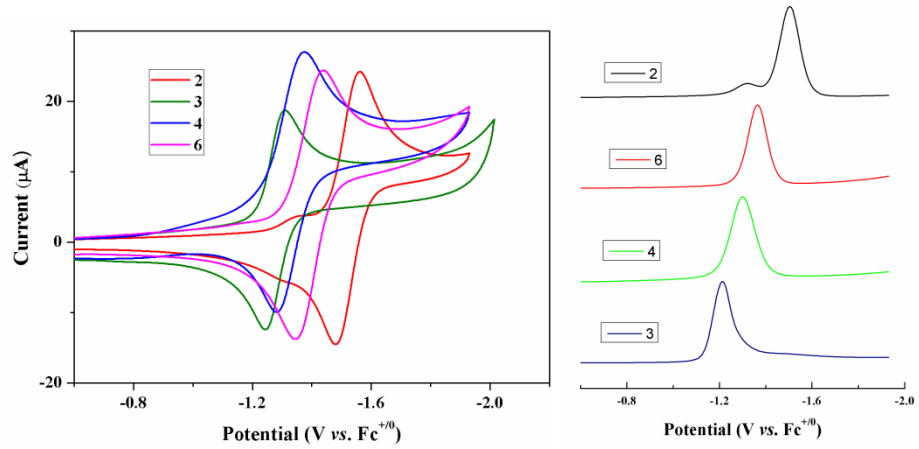

Figure 8. Cyclic voltammograms of UO_2L^2 (**2**) and $UO_2L^2 + M^+$ [M^+ = Li^+ (**3**), Na^+ (**4**), K^+ (**6**)] **(**left**)** which are recorded in actronitrile (0.1 M TBAP) at 100 mVs^{-1} scan rate and DPV of UO_2L^2 (**2**) and $UO_2L^2 + M^+$ [M^+ = Li^+ (**3**), Na^+ (**4**), K^+ (**6**)] **(**right**)** with a glassy carbon working electrode at 20 mVs^{-1} scan rate.

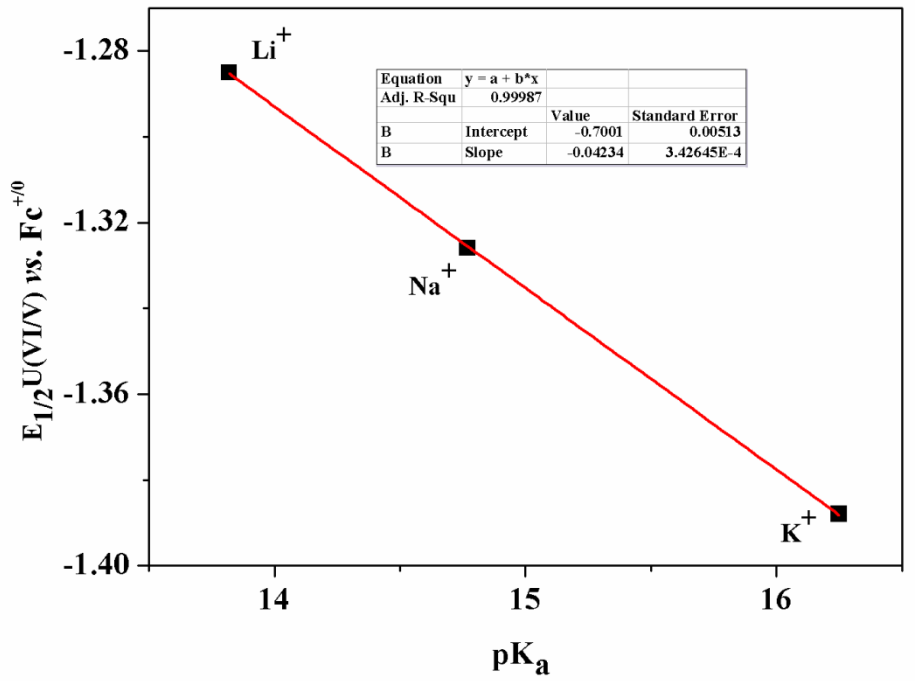

10.1002/chem.201904253

Figure 9. Dependence of half wave potentials ($E_{1/2}$) of the bimetallic complexes ($[(UO_2L^2)M]^{n+}$) *vs.* pK_a of $M(aqua)^{n+}$ ions as measure of their Lewis acidity.

Density Functional Theory (DFT) Studies.

The full geometries of the $[MLUO_2]^+$ series of complexes were optimized using DFT M06-2X/def2-TZVP level of theory without including counter-anion in the calculations. For uranium we have used the def2-SVP basis set, as implemented in TURBOMOLE. The optimized complexes are shown in Figure 10. The computed bond distances are in good agreement with those obtained in the X-ray data. The deviation of the bond distances for the Schiff-base ligand is less than 0.01 Å. There is a greater discrepancy (~0.2 Å) in the coordination distances, which are systematically longer in the computed structure. This is likely due to packing effects that are not considered in the calculations in addition to the absence of the counter ion, specially the coordinated nitrate anion and water molecule in the Ag complex that is responsible for the large discrepancy in coordination bond with the -OMe group (difference 0.2 Å). Moreover, in the K complex the discrepancies are likely due to the dimeric nature of the system in the solid state.

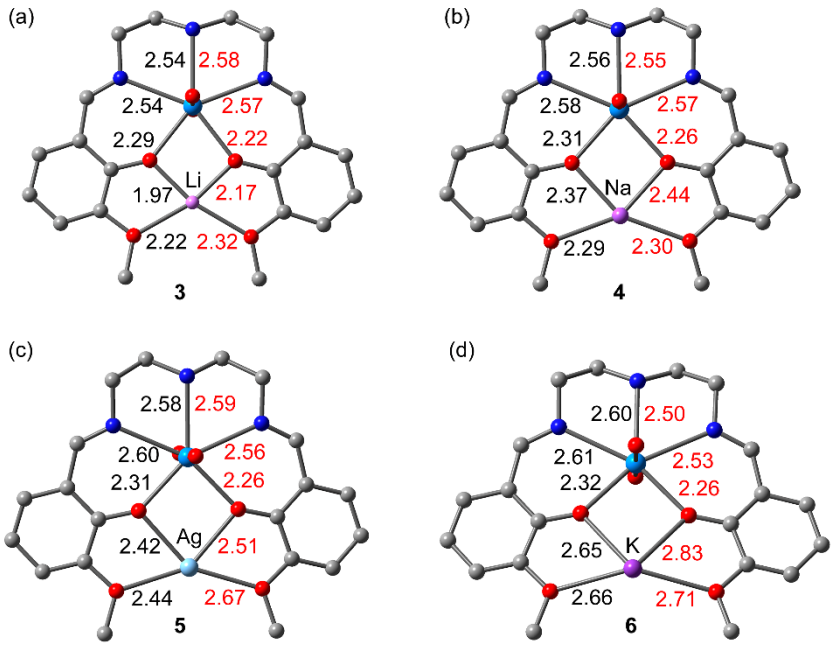

Figure 10. Optimized geometries of UO_2-M(I) complexes (M = Li, Na, K, and Ag). Distances in Å, values in black correspond to the theoretical and in red to the experimental ones (X-ray, mean distances).

In Table 1 we summarize the energy of the LUMO in M = Li, Na, K and Ag complexes. It is interesting to note that the reduction potential and LUMO energies exhibit a parallel behavior. The LUMO energies and plots have been obtained by performing energy calculations on the optimized M06-2X/def2-TZVP geometries at the M06-2X/SDD level of theory using Gaussian-16 program. In fact, we have found a strong linear correlation between the LUMO energy and the reduction potential (Ec), as shown in Figure 11 (R^2 = 0.9986), which gives reliability to the theoretical method and also suggests that these bimetallic complexes are monomeric in solution. The representations of the LUMOs are provided in Figure 12 and S29 (Supporting Information) for all complexes included in the regression plot along with the LUMO energies. In all cases the LUMO is composed by the $f_{zx^2-zy^2}$ atomic orbital at U with some contribution of the antibonding π orbital of the C=N bond.

Table 1. Experimental reduction potential, theoretical LUMO energy and Mulliken charge at the metal (q) corresponding to the optimized geometries shown in Figure. 10.

Complex	E_c U(VI/V) (mV)	E_{lumo} (eV)	q_M (e)
UO_2+K	-1.436	-3.5806	0.92
UO_2+Na	-1.391	-3.6494	0.83
UO_2+ Li	-1.328	-3.7356	0.62
UO_2+Ag	-1.361	-3.6883	0.64

10.1002/chem.201904253

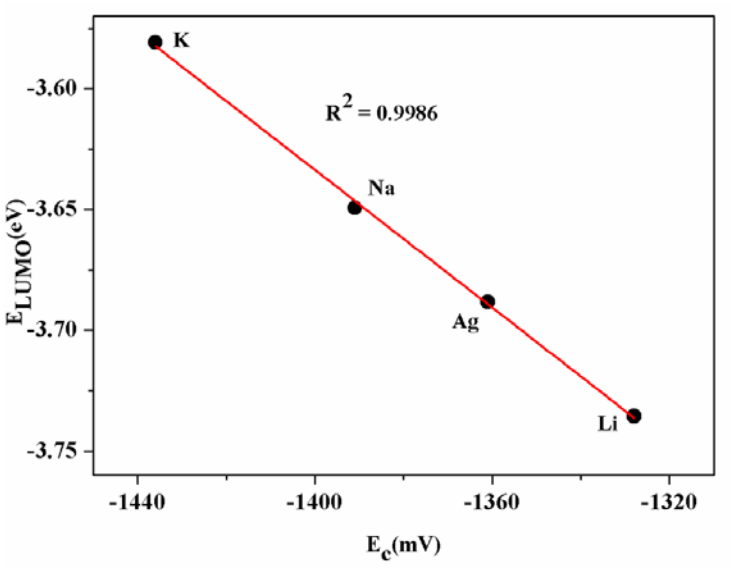

Figure 11. Correlation plot of E_{LUMO} *vs* Ec for Li(I), Na(I), K(I) and Ag(I) complexes.

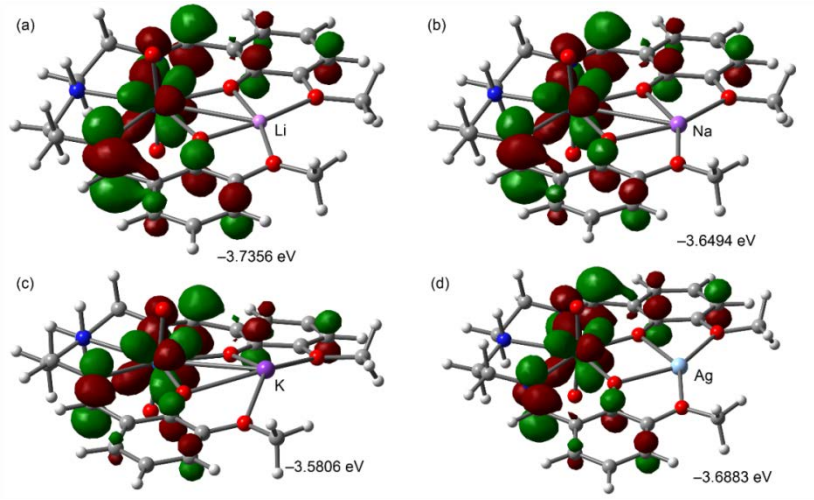

Figure 12. Plots of the LUMOs (0.04 a.u. isosurface) for Li, Na, K and Ag complexes.

In Table 1 we also summarize the electron charge of the cationic guest in the complexes. Interestingly the amount of positive charge at the guest metal also correlates with the experimental reduction potential. That is, the highest energetic LUMO and lowest value of reduction potential (–1436 mV) corresponds to K^+–complex that presents the largest atomic charge at the K^+ (0.92 e). Similarly, the lowest LUMO and highest value of reduction potential (–1328 mV) corresponds to the Li^+–complex that exhibits the lowest atomic charge (0.62 e). Therefore, the charge transference from the complex to the cation is larger in Li (around 0.48 e) than in K (only 0.08 e). This charge transfer is also related with the pKa correlation described above in Figure 9.

10.1002/chem.201904253

We have also optimized the complexes upon the one-electron reduction and computed the spin density plot, that is shown in Figure 13 for M = Li, Na, K and Ag complexes. The plot is very similar in all cases with the unpaired electron located on the U metal center. Some negative spin is delocalized onto the O atoms of the UO_2 moiety. The density plots obtained for the reduced species are similar to the shape of the LUMOs in the cationic compounds (represented in Figure 12).

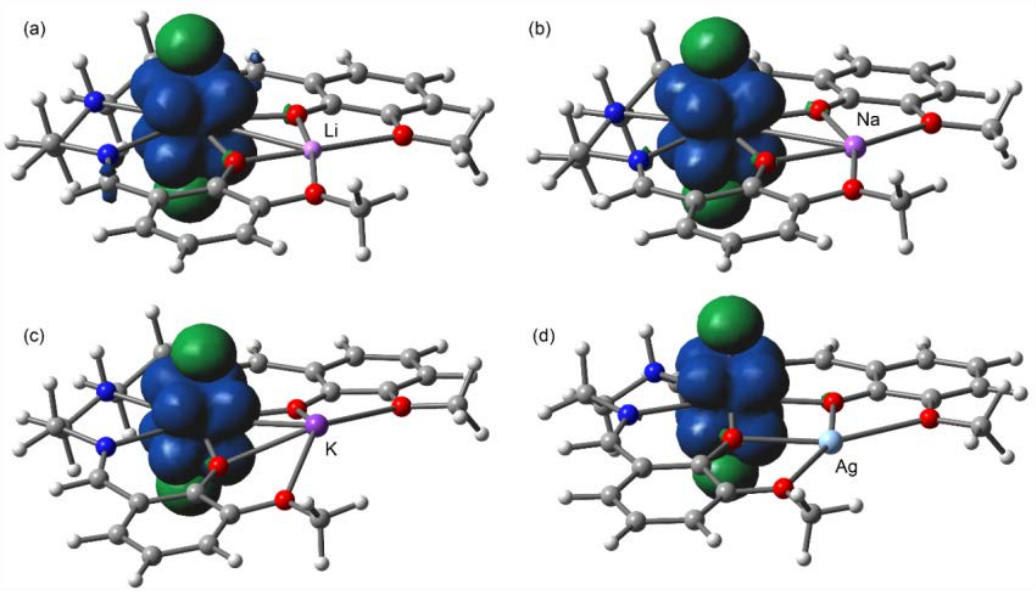

Figure 13. Spin density plots for the reduced species [U(V)O_2-M(I)] using the 0.001 isodensity.

Conclusions

We have shown here that the Schiff base ligands derived from the di-condensation of diethylenetriamine with *p*-vaniline (H_2L^1) or *o*-vaniline (H_2L^2) readily form complexes with U(VI) (**1** and **2** respectively) coordinating to the pentagonal basal plane of the uranyl ion through the N_3O_2 donor set of atoms. Both the complexes showed reversible U(VI)/U(V) couple on cyclic voltammetry in acetonitrile solution but a significant shift in reduction potential was only observed for **2** on addition of Li^+, Na^+, K^+ and Ag^+ to the solution. This shift in reduction potential is due to the inductive effect of the Lewis acidic metal ions, which pull the electron density from the uranyl centre to make it easily reducible from U(VI) to U(V). The correlation between Lewis acidic characters of metal ions (pK_a) with the reduction potentials of U(VI)/U(V) couple showed a linear relationship, and the DFT studies showed a

good agreement in this regard. The structural analyses revealed that in **2**, two phenoxido oxygen and two methoxy oxygen atoms are in close proximity to form a cavity. In the Na-adduct, the planarity and strong bonding of these four oxygen atoms indicate that the size of the cavity fit well to accommodate a sodium ion but too big for lithium ion as 50% of the cavity remained unoccupied in the Li-adduct. On the other hand, the Ag^+ and K^+ reside well above the mean plane of the four oxygen atoms indicating that these ions are too big compared to the size of the cavity. The other side of K^+ is so much exposed that four oxygen atoms of another unit are attached to form an 1:2 adduct. Complex **1** neither showed any shift of potential of U(VI)/U(V) couple nor any adduct was formed on addition of the same metal ions indicating the importance of the cavity for shift of the potential and formation of the adduct.

Experimental Section

Starting materials

All chemicals and solvents were of reagent grade and were commercially available. They were use without any further purification.

Synthesis of Schiff base ligands

H_2L^1 = *N,N′*-bis(5-methoxysalicylidene)diethylenetriamine) and H_2L^2 = *N,N′*-bis(3-methoxysalicylidene)diethylenetriamine)

The Schiff base ligand H_2L^1 was prepared by following method; 10 mmol (1.521 g) of 5-methoxysalicylaldehyde was mixed with 5 mmol (0.540 mL) of diethylenetriamine in methanol (25 mL). The resulting solution was refluxed for 3 h and then directly used for synthesis of complex **1**.

The Schiff base ligand H_2L^2 was synthesized in our laboratory by following the methods reported earlier.[50,51]

Synthesis of the complex $[UO_2L^1]$ (1)

A methanolic solution of Schiff base ligand H_2L^1 (0.5 mmol, 20 mL) was added to the acetronitrile solution (10 mL) of $UO_2(NO_3)_2 \cdot 6H_2O$ (0.250 g, 0.5 mmol), followed by triethylamine (1 mmol, 0.14 mL) with constant stirring. The resulting solution was stirred for 30 min and then kept in a desiccator. Red coloured single crystals of X-ray quality started to

appear inside the beaker, after 3-4 days which were separated by filtration after 6 days and dried in air.

Yield: 0.207 g (65%) $C_{20}H_{23}N_3O_6U$ (639.44) Calculated C, 37.57; H, 3.63; N, 6.57; Found C, 37.51; H, 3.55; N, 6.63; IR: $\nu_{(N–H)}$ = 3248 cm^{-1}, $\nu_{(C=N)}$ = 1632 cm^{-1}, $\nu_{(UO2)}$ asymmetric stretching) = 882 cm^{-1}. ESI-MS (positive ion mode, CH_3CN) calcd. *m/z* = 640.22; found at *m/z* = 640.45, which are assigned as $[UO_2L^1 + H]^+$. ^1H NMR (400 MHz, CD_3CN, ppm): δ 9.37 (s, 2H), δ 7.21 (dd, 2H), δ 7.06 (d, 2H), δ 6.91 (d, 2H), δ 4.64 (t, 2H), δ 4.52 (m, 2H), δ 4.14 (m, 2H), δ 3.76 (s, 6H), δ 3.52 (m, 2H).

Synthesis of complex $[UO_2L^2]\cdot CH_3CN\cdot CH_3OH$ (2)

Complex **2** was synthesized by following the same procedure as for complex **1**, using Schiff base ligand H_2L^2 (0.185 g, 0.5 mmol) insted of H_2L^1. Red coloured single crystals of X-ray quality appeared inside the beaker, which was separated out by filtration after 4-5 days.

Yield: 0.227 g (68%) $C_{21.25}H_{25.50}N_{3.5}O_{6.25}U$ (667.98). Calculated C, 38.21; H, 3.85; N, 7.34; Found C, 38.28; H, 3.77; N, 7.39; ; IR: $\nu_{(N–H)}$ = 3214 cm^{-1}, $\nu_{(C=N)}$ = 1625 cm^{-1}, $\nu_{(UO2}$ asymmetric stretching) = 883 cm^{-1}. ESI-MS (positive ion mode, CH_3CN) calcd. *m/z* = 662.20; found at *m/z* = 662.21, which are assigned as $[UO_2L^2 + Na]^+$. ^1H NMR (400 MHz, CD_3CN, ppm): δ 9.41 (s, 2H), δ 7.22 (dd, 2H), δ 7.14 (dd, 2H), δ 6.63 (t, 2H), δ 4.64 (m, 2H), δ 4.53 (m, 2H), δ 4.15 (m, 2H), δ 4.07 (s, 6H), δ 3.51 (m, 2H).

Synthesis of the complex $[UO_2L^2Li_{0.5}](ClO_4)_{0.5}$ (3), $[UO_2L^2Na(ClO_4)]_2$ (4), $[UO_2L^2AgNO_3(H_2O)]$ (5) and $[(UO_2L^2)_2K(H_2O)_2]PF_6$ (6). All the complexes **3–6** were prepared in a similar manner, by dissolving the complex **2** $[UO_2L^2]$ (0.334 g, 0.5 mmol) in acetronitrile solution (20 mL) and then solid $Li(ClO_4)\cdot 6H_2O$ (0.0532 g, 0.5 mmol) for **3**, $NaClO_4$ (0.0611 g, 0.5 mmol) for complex **4**, $AgNO_3$ (0.085 g, 0.5 mmol) for complex **5**, KPF_6 (0.046 g, 0.25 mmol) for **6** was added to it. The resulting solution was stirring for 15 min. For each case, diffraction quality red single crystals were obtained after a few days on slow diffusion of diethyl ether into the solution.

Complex 3. Yield 0.213 g (62%) $C_{20}H_{23}Cl_{0.5}Li_{0.5}N_3O_8U$ (688.65). Calculated C, 34.68; H, 3.35; N, 6.07; Found C, 34.72; H, 3.33; N, 6.14; IR: $\nu_{(N–H)}$ = 3197 cm^{-1}, $\nu_{(C=N)}$ = 1625 cm^{-1}, $\nu_{(UO2}$ asymmetric stretching) = 879 cm^{-1}, $\nu_{(ClO4)}$ = 1086 cm^{-1}. ESI-MS (positive ion mode, CH_3CN) calcd. *m/z* = 646.23; found at *m/z* = 646.23, which are assigned as $[UO_2L^2 + Li]^+$. ^1H

NMR (400 MHz, CD_3CN, ppm): δ 9.40 (d, 2H), δ 7.27 (dd, 2H), δ 7.17 (dd, 2H), δ 6.69 (t, 2H), δ 4.65 (t, 2H), δ 4.55 (m, 2H), δ 4.20 (m, 2H), δ 4.10 (s, 6H), δ 3.54 (m, 2H).

Complex 4. Yield 0.228 g (60%) $C_{20}H_{23}ClN_3NaO_{10}U$ (760.87). Calculated C, 31.53; H, 3.04; N, 5.52; Found C, 31.59; H, 2.96; N, 5.56; IR: $\nu_{(N-H)}$ = 3241 cm^{-1}, $\nu_{(C=N)}$ = 1631 cm^{-1}, $\nu_{(UO2}$ asymmetric stretching) = 898 cm^{-1}, $\nu_{(ClO4)}$ = 1089 cm^{-1}. ESI-MS (positive ion mode, CH_3CN) calcd. *m/z* = 640.22 and 662.20; found at *m/z* = 640.22 and 662.20 which are assigned as $[UO_2L^2 + H]^+$ and $[UO_2L^2 + Na]^+$ respectively. ^1H NMR (400 MHz, CD_3CN, ppm): δ 9.41 (s, 2H), δ 7.24 (d, 2H), δ 7.15 (d, 2H), δ 6.65 (t, 2H), δ 4.64 (t, 2H), δ 4.54 (m, 2H), δ 4.16 (m, 2H), δ 4.08 (s, 6H), δ 3.52 (m, 2H).

Complex 5. Yield 0.252 g (61%) $C_{20}H_{25}AgN_4O_{10}U$ (827.34). Calculated C, 29.03; H, 3.05; N, 6.77; Found C, 28.95; H, 3.01; N, 6.82; IR: $\nu_{(N-H)}$ = 3186 cm^{-1}, $\nu_{(C=N)}$ = 1627 cm^{-1}, $\nu_{(UO2}$ asymmetric stretching) = 892 cm^{-1}, $\nu_{(NO3)}$ = 1384 cm^{-1}. ESI-MS (positive ion mode, CH_3CN) calcd. *m/z* = 746.11; found at *m/z* = 746.12, which are assigned as $[UO_2L^2 + Ag]^+$. ^1H NMR (400 MHz, CD_3CN, ppm): δ 9.41 (s, 2H), δ 7.22 (dd, 2H), δ 7.14 (dd, 2H), δ 6.63 (t, 2H), δ 4.64 (t, 2H), δ 4.53 (m, 2H), δ 4.16 (m, 2H), δ 4.07 (s, 6H), δ 3.51 (m, 2H).

Complex 6. Yield 0.225 g (60%) $C_{40}H_{50}F_6KN_6O_{14}PU_2$ (1498.67). Calculated C, 32.05; H, 3.36; N, 5.61; Found C, 32.09; H, 3.31; N, 5.65; IR: $\nu_{(N-H)}$ = 3233 cm^{-1}, $\nu_{(C=N)}$ = 1629 cm^{-1}, $\nu_{(UO2}$ asymmetric stretching) = 872 cm^{-1}, $\nu_{(PF6)}$ = 845 cm^{-1}. ESI-MS (positive ion mode, CH_3CN) calcd *m/z* = 678.17 and 640.22; found at *m/z*, 678.58 and 640.59 which are assigned as $[UO_2L^2 + K]^+$ and $[UO_2L^2 + H]^+$ respectively. ^1H NMR (400 MHz, CD_3CN, ppm): δ 9.45 (s, 2H), δ 7.19 (d, 2H), δ 7.17 (d, 2H), δ 6.67 (t, 2H), δ 4.66 (m, 2H), δ 4.56 (m, 2H), δ 4.23 (m, 2H), δ 3.96 (s, 6H), δ 3.56 (m, 2H).

Physical measurements

Elemental analyses (C, H and N) were performed using a Perkin–Elmer 2400 series II CHN analyzer. IR spectra in KBr pellets (4000–400 cm^{-1}) were recorded using a Perkin-Elmer RXI FTIR spectrophotometer. The electronic absorption spectra (500–250 nm) in acetronitrile solution were collected in a Hitachi U-3501 spectrophotometer. ESI mass spectra were recorded on a WATERS Xevo G2-S QTof mass spectrometer in HRMS grade acetronitrile. ^1H NMR spectra were recorded in CD_3CN solvent for complexes **1**−**6** in a Bruker 400 MHz NMR instrument, where tetramethylsilane was used as an internal standard.

Electrochemical measurements

The electrochemical studies were performed using a Basi-Epsilon C3 Cell instrument at a scan rate of 50–400 mVs^{-1} within the potential range of 0 to –1.60 V vs. Ag/AgCl. Cyclic voltammograms were carried out using 0.1 MTBAP as supporting electrolyte and 1.0×10^{-3} M of complexes in acetronitrile solution which are deoxygenated by argon purging. The working electrode was a glassy carbon disk (0.32 cm^2) which was polished with alumina solution, washed with absolute acetone and accetronitrile, and air dried. The reference electrode was Ag/AgCl, with platinum as counter electrode. The potentials are given with respect to ferrocene/ferrocenium couple. All experiments were performed in standard electrochemical cells at 25°C.

X-ray Crystallographic data collection and refinement

Data for all complexes **1**–**6** were recorded on a Bruker-AXSSMART APEXII diffractometer equipped with a graphite monochromatorand Mo Kα (λ = 0.71073 Å) radiation. The crystals were positioned at 60 mm from the CCD. 360 frames were measured with a counting time of 10 s. The structures were solved using direct methods with the Shelxs97 program[52]. The non-hydrogen atoms were refined with anisotropic thermal parameters. The hydrogen atoms bonded to carbon were included in geometric positions and given thermal parameters equivalent to 1.2 times those of the atom to which they were attached. The hydrogen atoms bonded to oxygen and nitrogen were located in difference Fourier maps and refined with distance constraints. The structures were refined using Shelxl16-6[53] on F^2. In 3, the lithium ion and perchlorate anion were given occupancies of 50%. The perchlorate anion was disordered four-fold axis and was refined with distance constraints. Details of the crystallographic data for complexes **1**–**5** summarized in Table **2**. CCDC 1953884–1953888 contain the supplementary crystallographic data of complexes **1**–**5**, respectively for this paper and CCDC 1953891 is for complex **6** which is given in Supporting Information.

Theoretical methods

The full geometries of the $[MLUO_2]^+$ series of complexes were optimized using DFT M06-2X/def2-TZVP level of theory[54] without including counter-anion in the calculations. For uranium we have used the def2-SVP basis set, as implemented in TURBOMOLE v. 7.0 program[55], which has been used for the optimizations. The minimum nature of the

complexes was verified using frequency calculations. The orbital energies and plots were computed using the Gaussian-09 program[56] using the same functional and the SDD basis set[57].

Acknowledgements

T. K. G. is thankful to the University Grants Commission (UGC), New Delhi, for Senior Research Fellowship [Sr. no. 2061510191, Ref. no. 21/06/2015 (I) EU-V, dated 15/12/2015]. We thank USIC, The University of Burdwan, West Bengal, India, for providing the single-crystal X-ray diffractometer facility.

Keywords: U(VI) complexes • electrochemical study • bi-metallic complexes • theoretical investigations • crystal structure

References

[1] P. Wang, G. Liang, M. R. Reddy, M. Long, K. Driskill, C. Lyons, B. Donnadieu, J. C. Bollinger, C. E. Webster, X. Zhao, *J. Am. Chem. Soc*. **2018**, *140*, 9219−9229.

[2] A. Ourari, W. Derafa, D. Aggoun, *RSC Adv*. **2015**, *5*, 82894–82905.

[3] T. Chantarojsiri, A. H. Reath, J. Y. Yang, *Angew. Chem. Int. Ed*. **2018**, *57*, 14037–14042.

[4] S. K. Dey, A. Mukherjee, *Coord. Chem. Rev*. **2016,** *310*, 80–115.

[5] S. Fukuzumi, K. Ohkubo, *Coord. Chem. Rev*. **2010**, *254*, 372–385.

[6] B. E. Schultz, S. I. Chan, *Rev. Biophys. Biomol. Struct*. **2001**, *30*, 23–65.

[7] C. F. Yocum, *Coord. Chem. Rev*. **2008**, *252*, 296–305.

[8] E. Y. Tsui, R. Tran, J. Yano, T. Agapie, *Nature Chem.* **2013**, ***5***, 293–299.

[9] J. P. McEvoy, G. W. Brudvig, *Chem. Rev*. **2006**, *106*, 4455–4483.

[10] E. Y. Tsui, J. S. Kanady, T. Agapie, *Inorg. Chem*. **2013**, *52*, 13833−13848.

[11] J. Yano, V. Yachandra, *Chem. Rev*. **2014**, *114*, 4175−4205.

[12] Y. J. Park, S. A. Cook, N. S. Sickerman, Y. Sano, J. W. Ziller, A. S. Borovik, *Chem. Sci*. **2013**, *4*, 717–726.

[13] J. Park, Y. Morimoto, Y.-M. Lee, Y. You, W. Nam, S. Fukuzumi, *Inorg. Chem*. **2011**, *50*, 11612–11622.

[14] K. Sauer, J. Yano, V. K. Yachandra, *Coord. Chem. Rev*. **2008**, *252*, 318–335.

[15] S. Hong, Y.-M. Lee, M. Sankaralingam, A. K. Vardhaman, Y. J. Park, K.-B. Cho, T. Ogura, R. Sarangi, S. Fukuzumi, W. Nam, *J. Am. Chem. Soc*. **2016**, *138*, 8523−8532.

[16] Y. J. Park, J. W. Ziller, A. S. Borovik, *J. Am. Chem. Soc*. **2011**, *133*, 9258–9261.

[17] A. Kumar, D. Lionetti, V.W. Day, J. D. Blakemore, *Chem. Eur. J*. **2018**, *24*, 141–149.

[18] A. H. Reath, J. W. Ziller, C. Tsay, A. J. Ryan, J. Y. Yang, *Inorg. Chem*. **2017**, *56*, 3713−3718.

[19] P.-H. Lin, M.K. Takase, T. Agapie, *Inorg. Chem*. **2015**, *54*, 59−64.

[20] E. Y. Tsui, T. Agapie, *Proc. Nat. Acad. Sci. U.S.A.* **2013**, *110*, 10084–10088.

[21] V. Mougel, L. Chatelain, J. Pécaut, R. Caciuffo, E. Colineau, J.-C. Griveau, M. Mazzanti, *Nature Chem.* **2012**, *4*,1011–1017.

[22] L. Chatelain, F. Tuna, J. Pécaut, M. Mazzanti, *Dalton Trans*. **2017**, *46*, 5498–5502.

[23] R. Zhao, L. Mei, K.-q. Hu, M. Tian, Z.-f. Chai, W.-q. Shi, *Inorg. Chem*. **2018**, *57*, 6084−6094.

[24] N. Zhang, Y.-H. Xing, F-Y. Bai, *Inorg. Chem*. **2019**, *58*, 6866−6876.

[25] H. C. Hardwick, D. S. Royal, M. Helliwell, S. J. A. Pope, L. Ashton, R. Goodacre, C. A. Sharrad, *Dalton Trans.* **2011**, *40*, 5939–5952.

[26] B. E. Klamm, C. J. Windorff, C. Celis-Barros, M. L. Marsh, T. E. Albrecht-Schmitt, *Inorg. Chem.* **2019**, 10.1021/acs.inorgchem.9b00477.

[27] T. W. Hayton, G. Wu, *Inorg. Chem.* **2009**, *48*, 3065-3072.

[28] S. Das, Y. Oyola, R. T. Mayes, C. J. Janke, L.-J. Kuo, G. Gill, J. R. Wood, S. Dai, *Ind. Eng. Chem. Res*. **2016**, *55*, 4103−4109.

[29] C. W. Abney, R. T. Mayes, T. Saito, S. Dai, *Chem. Rev*. **2017**, *117*, 13935−14013.

[30] B. F. Parker, Z. Zhang, L. Rao, J. Arnold, *Dalton Trans*. **2018**, *47*, 639−644.

[31] P. L. Arnold, J. B. Love, D. Patel, *Coord. Chem. Rev*. **2009**, *253*, 1973−1978.

[32] C. J. Tatebe, J. J. Kiernicki, R. F. Higgins, R. J. Ward, S. N. Natoli, J. C. Langford, C. L. Clark, M. Zeller, P. Wenthold, M. P. Shores, J. R. Walensky, S. C. Bart, *Organometallics* **2019**, *38*, 1031−1040.

[33] C. Camp, V. Mougel, P. Horeglad, J. Pécaut, M. Mazzanti, *J. Am. Chem. Soc.***2010**, *132*, 17374–17377.

[34] E. J. Coughlin, Y. Qiao, E. Lapsheva, M. Zeller, E. J. Schelter, S. C. Bart, J. *Am. Chem. Soc*. **2019**, *141*, 1016−1026.

[35] X. Zhao, D. Zhang, Y. Ren, S. Chen, D. Zhao, *Eur. J. Inorg. Chem*. **2018**, 1185−1191.

[36] S. Fortier, T.W. Hayton, *Coord. Chem. Rev*. **2010**, *254*, 197−214.

[37] P. Horeglad, G. Nocton, Y. Filinchuk, J. Pécaut, M. Mazzanti, *Chem. Commun*. **2009**, 1843−1845.

[38] R. Faizova, S. White, R. Scopelliti, M. Mazzanti, *Chem. Sci*. **2018**, *9*, 7520–7527.

[39] M. Azam, S. I. Al-Resayes, G.Velmurugan, P. Venuvanalingam, J. Wagler, E. Kroke, *Dalton Trans*. **2015**, *44*, 568–577.

[40] K. Takao, S. Tsushima, S. Takao, A.C. Scheinost, G. Bernhard, Y. Ikeda, C. Hennig, *Inorg. Chem*. **2009**, *48*, 9602–9604.

[41] K. Takao, M. Kato, S. Takao, A. Nagasawa, G. Bernhard, C. Hennig, Y. Ikeda, *Inorg. Chem*. **2010**, *49*, 2349–2359.

[42] K. Mizuoka, S.-Y. Kim, M. Hasegawa, T. Hoshi, G. Uchiyama, Y. Ikeda, *Inorg. Chem*. **2003**, *42*, 1031–1038.

[43] K. Takao, Y. Ikeda, *Inorg. Chem*. **2007**, *46*, 1550–1562.

[44] M. Andruh, *Dalton Trans*. **2015**, *44*, 16633–16653.

[45] J. Long, R. Vallat, R. A. S. Ferreira, L. D. Carlos, F. A. A. Paz, Y. Guaria, J. Larionova, *Chem. Commun.* **2012**, *48*, 9974–9976.

[46] M. Andruh, *Chem. Commun.* **2011**, *47*, 3025–3042.

[47] T. D. Pasatoiu, J.-P. Sutter, A. M. Madalan, F. Z. C. Fellah, C. Duhayon, M. Andruh. *Inorg. Chem*. **2011**, *50*, 5890–5898.

[48] D. D. Perrin, Ionisation constants of inorganic acids and bases in aqueous solution, *Pergamon*, **1982**.

[49] S. Maity, S. Ghosh, A. Ghosh, *Dalton Trans*. **2019**, *48*, 14898–14913.

[50] T. K. Ghosh, S. Jana, A. Ghosh, *Inorg. Chem*. **2018**, *57*, 15216−15228.

[51] T. K. Ghosh, P. Mahapatra, S. Jana, A. Ghosh, *CrystEngComm*. **2019**, *21*, 4620−4631.

[52] G. M. Sheldrick, Shelxs97 *Acta Cryst*. **2008**, *A64*, 112.

[53] G.M.Sheldrick, Shelxl, *Acta Cryst*. **2015**, *C71*, 3−8.

[54] Y. Zhao, D.G. Truhlar, *Theor Chem Acc*. **2006**, *120*, 215–241.

[55] TURBOMOLE GmbH, available from http://www.turbomole.com.

[56] Gaussian 09, Revision D.01, M. J. Frisch, G. W. Trucks, H. B. Schlegel, G. E. Scuseria, M. A. Robb, J. R. Cheeseman, G. Scalmani, V. Barone, B. Mennucci, G. A. Petersson, H. Nakatsuji, M. Caricato, X. Li, H. P. Hratchian, A. F. Izmaylov, J. Bloino, G. Zheng, J. L. Sonnenberg, M. Hada, M. Ehara, K. Toyota, R. Fukuda, J. Hasegawa, M. Ishida, T. Nakajima, Y. Honda, O. Kitao, H. Nakai, T. Vreven, J. A. Montgomery, Jr., J. E Peralta, F. Ogliaro, M. Bearpark, J. J. Heyd, E. Brothers, K. N. Kudin, V. N. Staroverov, R. Kobayashi, J. Normand, K. Raghavachari, A. Rendell, J. C. Burant, S. S. Iyengar, J. Tomasi, M. Cossi, N. Rega, J. M. Millam, M. Klene, J. E. Knox, J. B. Cross, V. Bakken, C. Adamo, J. Jaramillo, R. Gomperts, R. E. Stratmann, O. Yazyev, A. J. Austin, R. Cammi, C. Pomelli, J. W. Ochterski, R. L. Martin, K. Morokuma, V. G. Zakrzewski, G. A. Voth, P. Salvador, J. J. Dannenberg, S. Dapprich, A. D. Daniels, Ö. Farkas, J. B. Foresman, J. V. Ortiz, J. Cioslowski, D. J. Fox, Gaussian, Inc., Wallingford CT, **2009**.

[57] T. H. Dunning Jr., P. J. Hay, in Modern Theoretical Chemistry, *Ed. H. F. Schaefer III*, *Vol. 3* (Plenum, New York, **1977**) 1−28.

10.1002/chem.201904253

Table 2: Crystallographic data and structure refinement of complexes **1**–**5**.

Compound	**1**	**2**	**3**	**4**	**5**
Chemical formula	$C_{20}H_{23}N_3O_6U$	$C_{21\cdot25}H_{25.50}N_{3.5}O_{6\cdot25}U$	$C_{20}H_{23}Cl_{0.5}Li_{0.5}N_3O_8U$	$C_{20}H_{23}ClN_3NaO_{10}U$	$C_{20}H_{25}AgN_4O_{10}U$
Formula weight	639.44	667.98	692.64	761.88	827.34
Crystal system	Orthorhombic	Monoclinic	Tetragonal	orthorhombic	Orthorhombic
Space group	*Pnma*	$P2_1$	*I4mcm*	*Pccn*	*Pbca*
a(Å)	10.0615(6)	10.3620(6)	20.8865(13)	20.281(6)	19.354(2)
b (Å)	24.6632(16)	11.2175(6)	20.8865(13)	21.469(6)	12.1934(14)
c (Å)	8.3400(5)	20.1552(11)	10.7830(7)	11.018(3)	20.284(2)
β (°)	90	91.618(2)	90	90	90
V (Å^3)	2096.6(2)	2341.8(2)	4704.0(7)	4797(2)	4768.8(10)
Z	4	4	8	8	8
ρ_{calc}(g cm^{-3})	2.052	3.256	1.945	2.107	2.296
T (K)	293(2)	296(2)	298(2)	293(2)	297(2)
μ (Mo Kα) (mm^{-1})	7.885	1.895	7.003	6.958	7.639
F(000)	1216	1278	2624	2904	3136
Reflections collected	26442	20807	38726	31542	44510
Independent reflections	1898	6926	2163	4386	4345
Reflections with I > 2σ(I)	1789	6355	1894	3360	2918
Final indices [$I>2\sigma(I)$]R_1[a], wR_2[b]	0.0296, 0.0657	0.0302, 0.0782	0.0303, 0.0735	0.0679,0.1491	0.0954, 0.1639
$R_{1[a]}$,$wR_{2[b]}$ [all data]	0.0320, 0.0668	0.0346, 0.0805	0.0394, 0.0810	0.0877,0.1601	0.1544,0.1863
GOF [c]	1.285	1.044	1.136	1.124	1.165
Residual electron Density, e/Å^{-3}	1.797, -2.881	1.010, -1.256	1.107,-0.965	3.555,-1.627	2.988,-3.392

[a]$R_1 = \sum||F_o|-|F_c||/\sum|F_o|$, [b]$wR_2$ $(F_o^2) = [\sum[w(F_o^2 - F_c^2)^2/\sum w F_o^4]^{½}$ and [c]$GOF = [\sum[w(F_o^2 - F_c^2)^2/(N_{obs} - N_{params})]^{½}$

10.1002/chem.201904253

Table of Contents Only

The effect of guest metal ions on the reduction potentials of uranium(VI) complexes: Experimental and theoretical investigations

Tanmoy Kumar Ghosh,[a] Prithwish Mahapatra,[a] Michael G. B. Drew,[b] Antonio Franconetti,[c] Antonio Frontera,[c]* Ashutosh Ghosh[a]*

A substantial shift of the reduction potential of U(VI)/U(V) couple in presence of guest metal ions. The DFT studies showed a good agreement with experimental results.